Polarization dependent optical absorption properties of single-walled carbon nanotubes and methodology for the evaluation of their morphology

Yoichi Murakami, Erik Einarsson, Tadao Edamura and Shigeo Maruyama*

Department of Mechanical Engineering, The University of Tokyo

7-3-1 Hongo, Bunkyo-ku, Tokyo 113-8656, Japan

Abstract

Polarization dependence of the optical absorption properties of SWNTs are presented and investigated in detail for the energy range 0.5 - 6 eV. We found that the absorption peaks in the UV region at approximately 4.5 and 5.25 eV exhibit remarkable and different dependencies on the morphology of the SWNT film, or equivalently, on the incident light polarization relative to the SWNT axis. An analytical pathway to evaluate the physical degree of SWNT alignment for a vertically aligned SWNT film is developed with both

* Corresponding Author. Tel & Fax: +81-3-5800-6983.
E-mail address: maruyama@photon.t.u-tokyo.ac.jp (S. Maruyama).

transition dipoles parallel and perpendicular to the SWNT axis taken into account. This analytical procedure, coupled with polarized optical absorption measurements performed on the vertically aligned SWNT film grown on substrates, leads to the determination of the bare optical absorption cross-section of SWNTs for both parallel and perpendicular to SWNT axis. In the end, the proposed methodology for evaluating the SWNT film morphology is applied to investigate the transient change of the degree of alignment in the growth process of our vertically aligned SWNT films.

Keywords:

A. carbon nanotubes; B. chemical vapor deposition; D. optical properties

1. Introduction

Since their discovery, single-walled carbon nanotubes (SWNTs) have been intensively studied because of their outstanding physical properties arising from their one-dimensional (1D) cylindrical structure formed by rolling up an sp^2-bonded graphene sheet [1]. The periodic boundary condition imposed in the circumferential direction gives rise to the quantization of electronic wave vectors in this direction and causes the divergences in the electronic density of states (eDOS) of SWNTs [2]. These divergences in the eDOS, known as van Hove singularities, produce discrete energy levels or "subbands", where the energy levels, as well as the distinction between metallic and semiconducting behavior, are determined solely by the SWNT's chirality [2]. Since the inter-subband gap corresponds to the energy of infrared to visible light and these subband gaps are tunable roughly by their diameter, SWNTs have been proposed for several optical applications, such as saturable absorbers for all-optic telecommunications devices [3-5], ultra-small infrared photoemission sources [6] or infrared photodetectors [7].

In order to utilize the 1D geometry of SWNTs that is preferable for polarization-sensitive optical devices, a sound understanding of the fundamental anisotropic optical properties of SWNTs is essential. However, very few experimental studies [8-10] have been performed

so far on the polarization dependent optical absorption properties of SWNTs that can provide direct confirmation of earlier theoretical studies [11-13]. From measurements on weakly aligned SWNTs in a gel matrix Islam et al. [8] reported optical absorption cross-sections for light polarized both parallel and perpendicular to the SWNT axis for the inter-subband energy region below 3.3 eV. Although they reported a smaller but non-zero absorption cross-section for cross-polarized light, the physical origins of these results as well as those of absorption baselines for the parallel-polarized light has not been presented [8]. Ichida et al. [9] measured optical absorption of aligned SWNTs in polymer films in which the baseline for cross-polarized light absorption was attributed to polarization-independent absorption by carbonaceous impurities. Namely, when calculating the degree of alignment they assumed that the light absorption by SWNTs was solely for polarization along the tube axis [9].

In determining the degree of physical ordering (or the *order parameter*) of the SWNTs, the above works [8,9] employed the scheme proposed by Gommans et al. [14] in which the polarization dependence of resonant Raman scattering (RRS) intensity was utilized assuming light polarized perpendicular to the SWNT axis is not absorbed. However, this assumption is not precisely correct for both inter-subband absorption [11,15,16] and

baseline absorption studied in this report. The use of this assumption for the determination of the order parameter is even not consistent to the result in Ref. 8 in which the absorption cross-section for cross-polarized light was actually non-zero.

Most importantly, the energy range investigated in these past studies [8-10] for the polarization dependent optical absorption properties of SWNTs was limited to below 3.5 eV, and properties in the higher energy region have not yet been studied. This is partly because the matrices used for the alignment of SWNTs in these studies absorb UV light. Since the absorption peaks at higher energy, including that regarded as the SWNT π-plasmon around 5 eV, produce broad absorption baselines in the inter-subband region at lower energy [17,18], a sound understanding of their fundamental properties and physical origins are extremely important.

In this report, we present and investigate in detail the polarization dependent optical absorption properties of SWNTs for the energy range 0.5 - 6 eV, by means of optical measurements on vertically aligned SWNT films grown on quartz substrates [19]. Specifically, we found that the absorption peaks at approximately 4.5 and 5.25 eV in the UV region exhibit remarkable and different behaviors depending on the morphology of the SWNTs, i.e., whether they are vertically aligned or 2-dimensionally (2D) random. This is a

direct indication that these UV light absorption peaks have strong dependence on the incident light polarization, which has been confirmed by polarized optical absorption measurements performed on the vertically aligned SWNT film [20].

Furthermore, in this paper, we present the analytical pathway to calculate the nematic order parameter (i.e., degree of physical alignment of the SWNTs) for the vertically aligned SWNT film by taking the multiple transition dipoles both parallel and perpendicular to SWNTs into account. As an output of this analytical procedure the intrinsic (bare) optical absorption cross-section of SWNTs is calculated for both light polarizations parallel and perpendicular to the SWNT axis. The proposed methodology for the evaluation of the SWNT film morphology is, at the end of this paper, applied to investigate the transient change of the degree of alignment through the CVD growth of our vertically aligned SWNT films.

2. Experimental and analysis procedure

The catalyst for the growth of SWNTs is supported by dip coating an optically polished quartz substrate (Fujitok Corp. #19983, 25 × 25 × 0.5 mm) into an ethanol solution containing dissolved Co-Mo bimetallic acetates (the amount of each metal species 0.01

wt%), as described in detail elsewhere (e.g. in Ref. 21). We have investigated the formation process as well as the morphology of the Co-Mo catalyst and revealed that this method yields finely monodispersed Co particles with diameter ranging from 1 - 2 nm at extremely high density (~ 1.3×10^{17} m^{-2}) on the substrate surface [19,22]. Thereby supported Co particles exhibited resistance to agglomeration at the CVD temperature (~ 800°C) being stabilized by an underlying $CoMoO_x$ compound layer formed on the SiO_2 surface [22].

SWNTs are grown by the alcohol catalytic CVD method [23,24]. First, the substrate on which catalyst is supported is placed inside our CVD apparatus [25]. After the vacuum of the chamber is checked, the chamber is heated up by an electric furnace with flowing 300 sccm of Ar/H_2 gas (3 % H_2) keeping the pressure of inside the chamber at 40 - 60 kPa. After approximately 30 min, when the furnace reaches 800°C, the valve to the vacuum pump is opened in full to bring the inside of the chamber to vacuum (~ 2 Pa). Ethanol vapor is subsequently introduced into the chamber at 10 Torr. The CVD reaction time in this report is 10 min unless otherwise specified.

Raman scattering measurements of prepared SWNTs are performed with a micro-Raman setup (Seki Technotron STR-250) that is composed of an optical microscope (Olympus BX51), a spectrometer (Chromex 501is), and a CCD (Andor DV401-FI). The light source

is a linearly polarized 488 nm (2.54 eV) Ar^+ laser. The measurement is performed in back-scattering configuration with a 50× objective lens. The incident laser power and laser spot size are 0.3 - 0.5 mW and 3 - 5 μm, respectively (≈ 3000 W/cm^2). The scattered light from the sample is collected back into the microscope passing through a depolarizer before being guided into the spectrometer.

Optical absorption measurements are performed with a UV-vis-NIR spectrophotometer (Shimadzu UV-3150) equipped with a rotational substrate holder located behind a UV-vis-NIR polarizer. The spot size of light on the sample surface is 3 × 15 mm. After baseline acquisition, we scan from 2500 nm (~ 0.5 eV) to 200 nm (~ 6 eV) at a specified angle to the sample holder (θ) and an incident polarization (s or p). The reference light path is remained blank. By convention, $\theta = 0$ means normal to the substrate, and the incident light is s-polarized (p-polarized) when its electric field vector is perpendicular (parallel) to the plane of incidence. It has been confirmed that the reflectance baseline of the bare quartz substrate for $0° < \theta < 45°$ is negligible, i.e. the contribution to the measured absorbance is less than 0.03 for p and 0.06 for s-polarizations, although correction for this contribution is made in the results below.

3. Growth and characterization of vertically aligned SWNT films

3.1 Characterization by microscopy

Figure 1 shows a typical vertically aligned SWNT film grown on a quartz substrate, taken at a fractured edge of the substrate by a Hitachi S-900 field-emission scanning electron microscope (FE-SEM) at 4 kV. The thickness of the film shown in Fig. 1 is 6 μm, and there is a film with approximately the same thickness on the opposite side of the substrate. Each string seen in the film's cross-section is a bundle of SWNTs. This SWNT film grown on quartz substrates is macroscopically uniform over the size of the substrate, based on its appearance and reflectance interferometry measurements of the film (not shown).

Figure 2 shows high-resolution transmission electron microscope (HR-TEM) images of the film obtained with a JEOL 2000EX at 120 kV. The sample was prepared by rubbing the film directly onto a TEM microgrid. The sample has not undergone dispersion in solvent in order not to destroy the morphology. Figure 2a shows part of the edge of a film section that retains its alignment as shown in the inset. The morphology seen in Fig. 2a coincides with the upper side of the films repeatedly observed by FE-SEM. Figures 2b and 2c show magnifications of the upper edge shown in Fig. 2a. These images indicate the SWNTs are clean, with virtually no amorphous, graphitic, or metallic impurities around the SWNTs. As

shown in the most magnified image in Fig. 2c, closed and empty SWNT ends are occasionally observed on this edge of the film.

During HR-TEM observations of such film sections, two types of edges were observed, one of them being shown in Figs. 2a - 2c. The other type of edge is shown in Fig. 2d, in which catalyst particles, seen as dark dots with diameters of 2 - 3 nm and presumably Co carbide, were found in abundance. This type of edge is considered to correspond to the interface between the film and the substrate. From these HR-TEM observations, the growth of the SWNT film here is considered to be base-growth from catalyst particles adhered to the substrate.

From measurements of diameters of more than 50 SWNTs, it was determined that the diameter of the sample ranges between 0.8 - 3.0 nm with average diameter $d_{av} \sim 2.0$ nm and standard deviation $\sigma \sim 0.4$ nm. No multi-walled carbon nanotubes (MWNTs) have been observed in repeated HR-TEM observations. A few double-walled carbon nanotubes (DWNTs) have been found so far, but their occurrence is negligible (well below 0.1 %) compared to that of SWNTs. Hence, the vertically aligned SWNT films examined in the following are clean SWNTs virtually free from impurities and multi-layered carbons, as confirmed by repeated HR-TEM observations on this type of SWNT sample.

3.2 Resonant Raman scattering analysis of SWNT films

RRS analysis is a strong tool for evaluating not only the quality and chiral distribution of SWNT samples but also their morphology. We have demonstrated that RRS spectra from vertically aligned SWNT films exhibit strong dependence on the polarization of incident light [26]. This polarization dependence has been considered to derive from the difference in selection rules between absorptions of light polarized parallel ($\Delta\mu = 0$) and perpendicular ($\Delta\mu = \pm 1$) to the SWNTs axis [11,15,16] (μ denotes the cutting line index of the 2D Brillouin zone of graphite [2]).

Figure 3 shows several RRS spectra from SWNT films measured with 488 nm laser light incident normal to the substrate plane. The upper panel shows the frequency region corresponding to the radial breathing mode (RBM) of SWNTs, on top of which a diameter scale based on the relationship "d / nm = 248 / (ν / cm^{-1})" [27] is shown. The lower panel of Fig. 3 presents the higher frequency region corresponding to the SWNT tangential mode including the D- (~ 1350 cm^{-1}) and G- (~ 1593 cm^{-1}) bands. The high quality of the samples is also confirmed from the high G-to-D ratio (> 25) in these spectra.

Figure 3a is a spectrum measured from a vertically aligned SWNT film that exhibits an RBM spectral shape characteristic of vertical aligned SWNT films [19,26]. A previous RRS study [26] revealed that the peaks at 145 and 180 cm^{-1}, marked with a '*', are dominant only when incident light polarization is perpendicular to the SWNT axis, and can be explained by quasi-nonvertical excitation of electrons between $\Delta\mu = \pm 1$ subbands. This implies that a specimen should exhibit different RBM spectra depending on the sample's morphology. Figure 3b shows an RRS spectrum measured from the same SWNT film used in Fig. 3a, but measured at a location where the film alignment was mechanically perturbed by tweezers. Apparently, the characteristic peaks at 145 and 180 cm^{-1} were suppressed and the shape of the spectrum looks very different from that in Fig. 3a. Furthermore, Fig. 3c shows a typical RBM spectrum measured from a 2-dimensionally (2D) random (i.e. grown in parallel to the substrate plane) SWNT film on a quartz substrate, whose corresponding FE-SEM and HR-TEM images are shown in Ref. 21. In this case, the characteristic peaks were suppressed and only peaks at 160 and 203 cm^{-1} that correspond to $\Delta\mu = 0$ inter-subband resonance are dominant. Although the difference between Figs. 3b and 3c partially arises from the difference in the diameter distribution (typically $d_{av} \sim 1.3$ nm for

the 2D random SWNTs [21]), dominance of the characteristic peaks at 145 and 180 cm^{-1} have never been observed for our 2D random SWNT films [21].

The alignment of a SWNT film can therefore be discerned to some extent from RBM spectra. However, since the RBM spectral shape of SWNTs is highly affected by their physical and chemical environment in addition to the power of the incident laser [26], a more stable and reproducible method for morphological evaluation is desirable. Although a measurement of the change of RRS intensity with changing incident light polarization and angle provides a rough measure to evaluate the degree of SWNT alignment in the sample [14], this is not a quick-and-easy method. Moreover, since SWNTs possess an intrinsic light absorption cross-section for cross-polarized light as presented below, quantitative separation of the contributions from cross-polarized light absorption to the obtained RRS intensity change is rather difficult. We will show in the following that optical absorption spectroscopy, which is generally easier than RRS measurement, provides a strong tool for distinguishing or even quantitatively evaluating the morphology of SWNT films.

3.3 Optical absorption spectrum of SWNT films

Prior to showing the light absorption spectrum of SWNT films, the effect of CVD chamber cleanness on the growth of SWNTs is briefly mentioned here. It has recently been found that the morphology as well as the growth speed of SWNTs strongly depends on the initial cleanness of the CVD chamber [28]. Namely, the speed of gas-desorption from the chamber wall is an important factor that controls the SWNT growth. Figure 4a shows optical absorption spectra of samples prepared at different gas-desorption rates V_{gd} [sccm] (cm^3/s expressed in the equivalent volumetric rate at standard state 1 atm, 0°C). The volume of our CVD chamber is approximately 1000 cm^3. The resultant morphology of the SWNT film ["vertically aligned" for (i) and (ii), or "2D random" for (iii)] is shown in parentheses. Figure 4a clearly shows the higher cleanness of the chamber is necessary for a higher degree of catalyst activity or larger amount of grown SWNTs, which ensures the vertically aligned growth [19]. We regard this vacuum deterioration mainly as gas desorption from the chamber wall because V_{gd} can be lowered by flushing the chamber under vacuum pump evacuation with several tens of sccm flow of Ar for a couple of hours, in addition to possible leakage of air into the chamber.

Figure 4b shows the optical absorption spectra for the same specimens (i – iii) as those shown in Fig. 4a but for a wider energy range (0.5 – 6 eV) on an arbitrary ordinate axis.

Spectrum (iv) is measured from a non-uniform SWNT film occasionally obtained in which vertically aligned regions and random regions co-exist in the same film. The morphology of the film is described along with each spectrum. The comparison of spectra (i – iv) presents that the absorption peaks approximately at 4.5 and 5.25 eV exhibit a clear dependence on the morphology of the SWNT film. That is, the feature at ~ 4.5 eV is dominant when the SWNTs are randomly oriented, while that at ~ 5.25 eV is dominant if the film is vertically aligned on the substrate, regardless of the average SWNT diameter. This strongly suggests that the SWNT film morphology could be reflected in an optical absorption spectrum around 5 eV, which is investigated in more depth in the next section.

4. Anisotropic optical absorption properties and analysis procedure

4.1 Polarization dependent optical absorption spectra and interpretation

Figure 5 shows polarization dependence of the absorption spectra of a vertically aligned SWNT film measured with s- (Fig. 5a) and p-polarized light (Fig. 5b) by changing the tilt angle θ from 0° to 45° at a step of 7.5° [20]. The absorbance is normalized by the $\cos^{-1}\theta$ increment of the light path length. The measured sample has a thickness of ~ 2.1 μm per

side (i.e. 4.2 μm in total because the film is grown on both sides of the substrate) and is identical to the sample "180 s" that is shown later in Fig. 9.

In the case of s-polarization (Fig. 5a), the spectra are independent of θ because of the dominant absorption of light by dipoles perpendicular to SWNT axis and weaker absorption by dipoles parallel to the axis, as confirmed below. In the case of p-polarization, on the other hand, the spectra show a clear anisotropy reflecting a dominance of absorption by dipoles parallel to SWNT axis as θ increases. These inter-subband absorption peak energies corresponds to the first (~0.64 eV) and second (~0.93 eV) inter-subband gaps of a semiconducting SWNT and the first gap (~1.45 eV) of a metallic SWNT with diameters of 1.85 - 1.90 nm [29], which coincides with the average diameter of the SWNTs measured from aforementioned HR-TEM observations.

In the higher energy region, it is noted that the two absorption peaks at approximately 4.5 and 5.25 eV exhibit clear dependence on the incident light polarization, with slight dispersions of ~ ± 0.1 eV by the direction of light polarization. This dispersion may be ascribed to the Coulomb interaction between neighboring SWNTs, as theoretically predicted by Shyu and Lin [13] using ideally aligned SWNTs with the same chirality.

Despite such slight dispersions in their energies, we refer to these peak locations as ~ 4.5 and 5.25 eV, respectively, hereafter.

These absorption peaks have been observed in several studies of randomly oriented SWNT films [17,18,30,31], but considerable disagreements are found among the discussions. Kataura et al. [17] attributed the peak at 4.5 eV to π-plasmon absorption observed in a purified SWNT film while the 5.2 eV peak was only seen in the pristine sample containing amorphous carbon. Pichler et al. [30] stated from their EELS measurements on purified SWNTs that the 5.2 eV peak observed at low electron momentum transfer was due to a π-plasmon along the SWNT axis. Reed and Sarikaya [31], however, performed EELS on purified SWNTs inside a TEM, and showed that a peak at 4.2-4.5 eV was measured for 'aloof' incidence of the electron beam, while the peak at ~5.2 eV was observed when the beam penetrated the center of an isolated SWNT. They explained these peaks as surface (4.2 - 4.5 eV) and bulk (~5.2 eV) π-plasmon excitations.

It is mentioned here that the absorption at ~ 4.5 eV is commonly observed in many graphitic materials [32-34]. It is known that the imaginary part of the dielectric function for graphite in the direction perpendicular to the *c*-axis $\mathrm{Im}\{\varepsilon_{\perp}\}$ has a maximum at 4.5 eV [35,36] whereas the maximum of the EELS function in the same direction $\mathrm{Im}\{-\varepsilon_{\perp}^{-1}\}$ is

found at ~ 7 eV [35,36]. In the direction parallel to the *c*-axis, however, the optical properties of graphite have not yet been fully elucidated because of difficulties in preparing good optical surfaces parallel to the *c*-axis [35,37]. Nevertheless, according to EELS data obtained by Venghaus [38], the maximum in $\mathrm{Im}\{-\varepsilon_{\parallel}^{-1}\}$ appears at ~5.2 eV and a broad maximum in $\mathrm{Im}\{\varepsilon_{\parallel}\}$ is found at ~ 4.0 eV [35,36].

Based on the fact that these two peaks are observed at almost the same positions (~ ± 0.1 eV) regardless of the diameter or preparation method of SWNT samples (Fig. 4b and Refs. 17, 18, 30, and 31), it is reasonably deduced that the observed peaks at ~ 4.5 and 5.25 eV in Fig. 5 originate from the anisotropic optical properties of graphitic plane. They are attributed to the maxima in $\mathrm{Im}\{\varepsilon_{\perp}\}$ (parallel to the SWNT axis) and $\mathrm{Im}\{-\varepsilon_{\parallel}^{-1}\}$(perpendicular to the SWNT axis), respectively. It is noted that similar polarization behavior of the absorption peaks at ~ 4.5 and 5.25 eV in the present study are seen in Ref. 39 in which a purified HiPco SWNT thin-film aligned on a glass plate was measured. Although no mention was given by the authors, their results are consistent with the present discussion.

Above results and discussions indicate that this polarization dependence around 5 eV is practically useful for the evaluation of SWNT morphology. Namely, these absorption structures at ~ 4.5 and 5.25 eV not only give a method for distinction between random and

aligned SWNT film morphologies, but also a useful foothold for quantitatively evaluating the degree of SWNT alignment as shown in the following subsection.

4.2 Modeling and formulation of the optical absorption anisotropy

The optical absorption anisotropy and intrinsic (or "bare") optical cross-section of SWNTs are derived based on the result shown in Fig. 5b. First, an *x*-*y*-*z* Cartesian coordinate system is defined so that the *z*-axis is normal to the substrate and the light propagation vector $\boldsymbol{k}$ lies in the *y*-*z* plane as illustrated in Fig. 6. The angle between $\boldsymbol{k}$ and the *z*-axis is $\theta\,(0 \le \theta \le \pi/2)$, as defined previously. The orientation of the SWNT axis vector $\boldsymbol{l}$ is described by $\varphi\,(0 \le \varphi \le \pi/2)$ as a deviation angle of $\boldsymbol{l}$ from the *z*-axis, and by $\psi\,(0 \le \psi \le 2\pi)$ as a rotational angle of a plane constructed by the $\boldsymbol{l}$ and *z*-axes from the *z*-*x* plane. A SWNT is assumed to have a collinear dipole moment $\boldsymbol{\mu}_{\parallel}$ parallel to $\boldsymbol{l}$ and a non-collinear dipole moment $\boldsymbol{\mu}_{\perp}$ perpendicular to $\boldsymbol{l}$. Since $\boldsymbol{\mu}_{\perp}$ has all components around $\zeta\,(0 \le \zeta \le 2\pi)$, a dipole located at the circumferential angle ζ is expressed as

$$\boldsymbol{\mu}_{\perp} = \boldsymbol{\mu}_{\perp(\zeta=0)} \cos\zeta + \boldsymbol{\mu}_{\perp(\zeta=\pi/2)} \sin\zeta \qquad (1)$$

Here, $\boldsymbol{\mu}_{\parallel}$, $\boldsymbol{\mu}_{\perp(\zeta=0)}$ and $\boldsymbol{\mu}_{\perp(\zeta=\pi/2)}$ are written as

$$\boldsymbol{\mu}_{\parallel} = \mu_{\parallel}\begin{pmatrix} -\sin\varphi\cos\psi \\ \sin\varphi\sin\psi \\ \cos\varphi \end{pmatrix},\quad \boldsymbol{\mu}_{\perp(\zeta=0)} = \mu_{\perp}\begin{pmatrix} \sin\psi \\ \cos\psi \\ 0 \end{pmatrix},\quad \boldsymbol{\mu}_{\perp(\zeta=\pi/2)} = \mu_{\perp}\begin{pmatrix} \cos\varphi\cos\psi \\ -\cos\varphi\sin\psi \\ \sin\varphi \end{pmatrix} \tag{2}$$

Since electronic vectors for s- and p-polarization are written as $\boldsymbol{E}_{\mathrm{s}} = E(1\ 0\ 0)^{\mathrm{T}}$ and $\boldsymbol{E}_{\mathrm{p}} = E(0\ \cos\theta\ \sin\theta)^{\mathrm{T}}$, respectively, absorbance of s-polarized light by collinear dipoles $\Lambda^{\mathrm{S}}{}_{\parallel}(\varphi)$ is expressed as

$$\Lambda^{\mathrm{S}}{}_{\parallel}(\varphi) = \left|\boldsymbol{\mu}_{\parallel}\cdot\boldsymbol{E}_{\mathrm{S}}\right|^2 = \frac{1}{2}\mu_{\parallel}{}^2E^2\sin^2\theta \tag{3}$$

where the relationships

$$\Lambda^{\mathrm{S}}{}_{\parallel}(\varphi,\psi) = \frac{\int_{-\pi}^{\pi}\Lambda^{\mathrm{S}}{}_{\parallel}(\varphi,\psi,\zeta)d\zeta}{\int_{-\pi}^{\pi}d\zeta},\quad \Lambda^{\mathrm{S}}{}_{\parallel}(\varphi) = \frac{\int_{-\pi}^{\pi}\Lambda^{\mathrm{S}}{}_{\parallel}(\varphi,\psi)d\psi}{\int_{-\pi}^{\pi}d\psi} \tag{4}$$

were used. Actually, φ has some distribution described by an unknown function $f(\varphi)$, [40] resulting in the experimentally observed $\Lambda^{\mathrm{S}}{}_{\parallel}$' to be expressed as

$$\Lambda^{\mathrm{S}}{}_{\parallel}' = \frac{\int_0^{\frac{\pi}{2}} f(\varphi)\cdot\Lambda^{\mathrm{S}}{}_{\parallel}(\varphi)d\varphi}{\int_0^{\frac{\pi}{2}} f(\varphi)d\varphi} = \frac{1}{2}\mu_{\parallel}{}^2E^2 < \sin^2\varphi > \tag{5}$$

Similarly for the absorbance of s-polarized light by non-collinear dipoles $\Lambda^{\mathrm{S}}{}_{\perp}$' is written as

$$\Lambda^{\mathrm{S}}{}_{\perp}' = \frac{\int_0^{\frac{\pi}{2}} f(\varphi)\cdot\Lambda^{\mathrm{S}}{}_{\perp}(\varphi)d\varphi}{\int_0^{\frac{\pi}{2}} f(\varphi)d\varphi} = \frac{1}{4}\mu_{\perp}{}^2E^2(1+ < \cos^2\varphi >) \tag{6}$$

Therefore, absorbance of s-polarized light by all dipoles measured by experiment Λ^{S}' is

$$\Lambda^{S}{}' = \frac{1}{2}\Lambda_{0,\|} < \sin^2\varphi > + \frac{1}{2}\Lambda_{0,\perp}(1 + < \cos^2\varphi >) \tag{7}$$

where we defined $\mu_{\|}{}^2 E^2 \equiv \Lambda_{0,\|}$ and $\mu_{\perp}{}^2 E^2 \equiv 2\ \Lambda_{0,\perp}$. Since the Λ^{S}' is a function only of φ, the baseline is constant regardless of θ, consistent with the observation in Fig. 5a.

Similarly, absorbance of p-polarized light by all dipoles measured by experiment Λ^{P}' is derived to be

$$\begin{aligned}\Lambda^{P}{}'(\theta) = \frac{1}{2}\Lambda_{0,\|}(\cos^2\theta < \sin^2\varphi > + 2\sin^2\theta < \cos^2\varphi >) \\ + \frac{1}{2}\Lambda_{0,\perp}\left\{\cos^2\theta(1 + < \cos^2\varphi >) + 2\sin^2\theta < \sin^2\varphi >\right\}\end{aligned} \tag{8}$$

However, experimentally obtainable values are $\Lambda'_{(\theta=0)}$ and $\Lambda'_{(\theta=\pi/2)}$, which are expressed using Eq. 8 as

$$\Lambda'_{(\theta=0)} \equiv \Lambda^{P}{}'(0) = \Lambda^{S}{}' = \frac{1}{2}\Lambda_{0,\|} < \sin^2\varphi > + \frac{1}{2}\Lambda_{0,\perp}(1 + < \cos^2\varphi >) \tag{9}$$

$$\Lambda'_{(\theta=\pi/2)} \equiv \Lambda^{P}{}'(\pi/2) = \Lambda_{0,\|} < \cos^2\varphi > + \Lambda_{0,\perp} < \sin^2\varphi > \tag{10}$$

The relation of total absorbance is satisfied by these equations because $\Lambda_0 = 2\ \Lambda_{0,\perp} + \Lambda_{0,\|} = 2\ \Lambda'_{(\theta=0)} + \Lambda'_{(\theta=\pi/2)}$. Using Eqs. 9 and 10, the anisotropy α in the case of multiple dipole absorption is expressed as

$$\alpha \equiv \frac{\Lambda'_{(\theta=\pi/2)} - \Lambda'_{(\theta=0)}}{\Lambda'_{(\theta=\pi/2)} + 2\Lambda'_{(\theta=0)}} = \frac{\Lambda_{0,\|} - \Lambda_{0,\perp}}{\Lambda_{0,\|} + 2\Lambda_{0,\perp}} \cdot \frac{1}{2}\left(3 < \cos^2\varphi > -1\right) \tag{11}$$

where the right side of the right-most term is the nematic order parameter *S*, defined as [40]

$$S \equiv \frac{1}{2}\left(3 < \cos^2 \varphi > -1\right) \tag{12}$$

4.3 Determination of optical anisotropy and the absorption cross-section

Solid lines shown in Fig. 7a are the lower energy portion of Fig. 5b (0.5 - 3 eV). Since the absorbance increases according to $\sin^2\theta$ at each energy point, these spectra are readily extrapolated to the absorbance at θ = 90°, which is shown as a dashed line. Hence the spectra at θ = 0° and 90° in Fig. 7a are $\Lambda'_{(\theta=0)}$ and $\Lambda'_{(\theta=\pi/2)}$, respectively, defined in Eqs. 9 and 10.

Figure 7b shows α for 0.5 - 3 eV calculated using Eq. 11. It is recognized that α becomes larger in the lower energy region (< 2 eV) because the collinear absorption by $\Delta\mu$ = 0 inter-subband transition (E^S_{11}, E^S_{22} and E^M_{11}) is dominant in this region. In contrast, a smaller value of α in the higher energy region is explained by the enhancement of optical absorption by the non-collinear dipoles perpendicular to the SWNT axis, as presented later.

In order to determine the SWNT bare optical cross-section for both parallel ($\sigma_{\parallel}$) and perpendicular ($\sigma_{\perp}$) polarizations, one must first determine the order parameter *S*. However, this cannot be determined at this point from Fig. 7 because these parameters are related to each other as

$$\alpha = \frac{\sigma_{\parallel} - \sigma_{\perp}}{\sigma_{\parallel} + 2\sigma_{\perp}} \cdot S \tag{13}$$

using Eq. 11 and Beer-Lambert law. Therefore, to find *S*, it is necessary to separate the dependence of collinear dipoles on polarization from other dipoles. As recognized from Fig. 5b, the collinear absorption peak at ~ 4.5 eV exhibits the clearest dependence on incident light polarization. We performed a Lorentzian curve fitting on the result shown in Fig. 5b for 2.5 - 6 eV based on the observed absorption maxima of either Im{ε} or Im{-ε^{-1}} approximately at 2.8, 4.0, 4.4, and 5.2 eV reported by Lee et al. [41] from their reflectance measurements of SWNT films.

Figure 8a shows the decomposed spectra obtained by setting four peaks at {2.8, 4.0, 4.5, and 5.3} ± 0.1 eV. Their widths were fixed at {4.00, 1.30, 0.98, and 1.72} ± 0.02 eV, respectively. We have confirmed that the same peak positions and widths also decompose the absorption spectra of other SWNT films with different morphologies and diameters. Figure 8b exemplifies the Lorentzian fitting for an absorption spectrum of a 2D random SWNT film identical to that shown in Fig. 4(iii). Since the majority of SWNTs in our 2D random SWNT film have diameters ranging from 1.1 - 1.7 nm [21], which is smaller than the diameter of the present vertically aligned SWNT film, it is confirmed that absorption spectra of SWNT films are consistently fitted according to this method regardless of

diameter and morphology. It is, however, mentioned that the origins of peaks located at ~ 2.8 and 4.0 eV have not yet been convincingly clarified.

Since Fig. 8a shows that the peak at 4.5 eV exhibits the clearest dependence on θ, it is used for the determination of S. From the change of amplitude of the peak at 4.5 eV, which is well fitted with {baseline + $\sin^2\theta$}, $S \approx 0.75$ and $\langle\varphi\rangle \approx 24°$ are calculated using Eqs. 11 and 13.

The molar absorption cross-sections of examined SWNT films for light polarized parallel ($\eta_{\parallel}$) and perpendicular to the z-axis ($\eta_{\perp}$) are directly determined from Fig. 5b (or Fig. 7a) using the density of C atoms of ~3.0×10^{-3} mol/cm^3, which was determined by comparing the weight of the substrate measured by a precision electric microbalance before and after removing the film from the substrate. Here, we have defined η based on the definition of absorbance $\Lambda = -\log_{10}T = \eta \cdot n \cdot l$ in which T, n, l are optical transmission, molar concentration of C, and film thickness, respectively. Therefore, we can calculate the bare optical absorption cross-sections of the SWNTs in the directions parallel ($\sigma_{\parallel}$) and perpendicular to the SWNT axis ($\sigma_{\perp}$) using the following relationships derived using Eqs. 9 - 12.

$$\sigma_{\parallel} = \frac{1}{3}\left\{2\eta_{\perp} + \eta_{\parallel} + \frac{2(\eta_{\parallel} - \eta_{\perp})}{S}\right\} \tag{14}$$

$$\sigma_{\perp} = \frac{1}{3}\left(2\eta_{\perp} + \eta_{\parallel} - \frac{\eta_{\parallel} - \eta_{\perp}}{S} \right) \tag{15}$$

Figure 8c shows $\sigma_{\parallel}$ and $\sigma_{\perp}$ calculated with Eqs. 14 and 15 for 0.5 - 6 eV in unit of Å^2 / atom C. In the lower energy region below 3 eV, $\sigma_{\parallel}$ shows the inter-subband absorption structure by the $\Delta\mu$ = 0 transition while $\sigma_{\perp}$ shows a monotonous baseline with lower magnitude. On the other hand, in the higher energy region, $\sigma_{\parallel}$ and $\sigma_{\perp}$ have maxima at ~ 4.5 and 5.25 eV respectively, as expected from the result of Fig. 5. The magnitudes of $\sigma_{\parallel}$ and $\sigma_{\perp}$ at 2.5 eV in Fig. 8c are approximately 30 % and 55 % smaller, respectively, than those shown by Islam et al. [8].

Most importantly, Fig. 8c shows that in the energy region < 3 eV, often the focus of both fundamental and applied studies, there exists a small but appreciable baseline of $\sigma_{\perp}$. This baseline comes from the non-collinear π-plasmon absorption at ~ 5.25 eV extending into the lower energy region, and therefore is an intrinsic optical property of SWNTs originating from the corresponding property of graphite. Therefore, it is important to recognize that the optical absorption properties of SWNTs have contributions not only from ordinary inter-subband transitions, but also from the absorption properties of graphitic plane around 5 eV for light polarized both parallel and perpendicular to the SWNT axis.

5. Investigation of the growth and alignment process of the SWNT film

The findings obtained above are employed in the investigation of the alignment process of the SWNT films grown by current method. First, a series of CVD experiments were performed, changing the CVD reaction time while keeping all other conditions the same, including the gas desorption rate discussed in Fig. 4a. In this series of experiments, the reaction temperature and ethanol vapor pressure were 800°C and 10 Torr, respectively. Figure 9 shows a cross-sectional FE-SEM image of the SWNT film after various CVD times from 15 to 600 s [28]. This figure reveals the growth process of the SWNT film from 15 s, when the film is a mixture of random SWNTs in the upper portion and weakly aligned SWNTs in the lower portion, to 600 s, where the alignment has been well established.

The morphological change with CVD time is more quantitatively evaluated by optical absorption spectra measured normal to the substrate plane ($\theta = 0$). Figure 10a shows the absorbance at 2.54 eV divided by the thickness of the SWNT film determined from FE-SEM observations (ordinate) vs. CVD time (abscissa). It is recognized that the absorbance at 2.54 eV per unit film thickness monotonically decreases with the progress of CVD time. This represents the process of alignment of the film from a near-random state to

an aligned state, from which it is understood that the alignment is established within the time of 30 - 100 s.

Furthermore, the optical absorption spectra of these samples are decomposed into Lorentzian curves as performed in Fig. 8, and the magnitudes of the peaks at 4.5 and 5.25 eV are compared. Figure 10b shows the magnitude ratio of the 4.5 and 5.25 eV peaks ($I_{4.5eV}/I_{5.25eV}$) plotted against CVD time, obtained by the Lorentz decomposition of corresponding optical absorption spectra. This result also demonstrates that the characteristic absorption peaks near 5 eV can give a convenient measure for the quantitative evaluation of the degree of SWNT alignment, in addition to quick measurement for the qualitative distinction between random and aligned morphologies as demonstrated in Fig. 4b.

6. Conclusion

We have presented polarization dependent optical absorption properties of SWNTs through detailed optical measurements and analysis of SWNT films directly grown on quartz substrates. It was found that the absorption at approximately 4.5 and 5.25 eV in the UV region exhibit remarkable dependences on the morphology of SWNT films, or

equivalently, on the polarization of incident light. From the experimental results, considered with past experimental data for both SWNTs and graphite, we have deduced that these absorption peaks at ~ 4.5 and 5.25 eV originate from the maxima in $\mathrm{Im}\{\varepsilon_{\perp}\}$ and $\mathrm{Im}\{-\varepsilon_{\parallel}^{-1}\}$ of the graphitic plane, which correspond to orientations parallel and perpendicular to the SWNT axis, respectively. Practically, the UV absorption spectrum of a SWNT film provides a convenient measure to discern its morphology, as shown in Fig. 4b, instead of laborious cross-sectional SEM observation of the SWNT film.

Based on experimental observations, we have developed an analytical pathway to evaluate the nematic order parameter of an SWNT film utilizing dependence of the collinear absorption peak at ~ 4.5 eV on incident light polarization. This analytical procedure, coupled with polarized optical absorption measurements performed on the vertically aligned SWNT film, lead to the determination of the bare optical absorption cross-section of the SWNTs. The methodology proposed in this work successfully describes the transient change of the degree of physical alignment during the growth process of our vertically aligned SWNTs.

The remarkable anisotropic optical absorption of SWNTs revealed in this report suggests the possibility of innovative optical applications of SWNTs, such as polarization-sensitive

saturable absorbers or passive optical UV switches. Moreover, the optical relevance between SWNTs and graphite above the inter-subband region (> 3 eV) implies the important possibility of studying the optical properties of graphite, which has not yet been fully elucidated in the direction of the *c*-axis, by studying aligned SWNTs as arrays of graphene cylinders.

Acknowledgement

Part of this work was financially supported by JSPS #16360098 and #1610754 and KAKENHI #13GS0019 from MEXT. The authors thank Prof. T. Okubo and Mr. T. Sugawara at UT for the use of Hitachi FE-SEM S-900, Mr. T. Nishii and Mr. N. Masuyama at J-Power Co. Ltd. for the use of Hitachi FE-SEM S-4700, and Dr. H. Tsunakawa at UT for the support in our TEM observation. The part of the measurement in this work is owed to Mr. S. Chiashi and Mr. K. Miyake at UT.

References

[1] Iijima S, Ichihashi T. Single-shell carbon nanotubes of 1-nm diameter. Nature 1993; 363(6430): 603-605

[2] Saito R, Dresselhaus G, Dresselhaus MS. Physical Properties of Carbon Nanotubes, London: Imperial College Press, 1998.

[3] Chen YC, Raravikar NR, Schadler LS, Ajayan PM, Zhao YP, Lu TM, et al. Ultrafast optical switching properties of single-wall carbon nanotube polymer composites at 1.55 μm. Appl Phys Lett 2002; 81(6): 975-977

[4] Sakakibara Y, Tatsuura S, Kataura H, Tokumoto M, Achiba Y. Near-infrared saturable absorption of single-wall carbon nanotubes prepared by laser ablation method. Jpn J Appl Phys 2003; 42(5A): L494-L496

[5] Yamashita S, Inoue Y, Maruyama S, Murakami Y, Yamaguchi H, Jablonski M, et al. Saturable absorbers incorporating carbon nanotubes directly synthesized onto substrates and fibers and their application to mode-locked fiber lasers. Opt Lett 2004; 29(14): 1581-1583

[6] Misewich JA, Martel R, Avouris P, Tsang JC, Heinze S, Tersoff J. Electrically induced optical emission from a carbon nanotube FET. Science 2003; 300(5620): 783-786

[7] Freitag M, Martin Y, Misewich JA,Martel R, Avouris P. Photoconductivity of single carbon nanotubes. Nano Lett 2003; 3(8): 1067-1071

[8] Islam MF, Milkie DE, Kane CL, Yodh AG, Kikkawa JM. Direct measurement of the polarized optical absorption cross section of single-wall carbon nanotubes. Phys Rev Lett 2004; 93(3): 037404-1-037404-4

[9] Ichida M, Mizuno S, Kataura H, Achiba Y, Nakamura A. Anisotropic optical properties of mechanically aligned single-walled carbon nanotubes in polymer. Appl Phys A 2004; 78(8): 1117-1120

[10] Hwang J, Gommans HH, Ugawa A, Tashiro H, Haggenmueller R, Winey KI, et al. Polarized spectroscopy of aligned single-wall carbon nanotubes. Phys Rev B 2000; 62(20): R13310-R13313

[11] Ajiki H, Ando T. Aharonov-Bohm effect in carbon nanotubes. Phys B 1994; 201: 349-352

[12] Lin MF, Chuu DS. pi plasmons in carbon nanotube bundles. Phys Rev B 1998; 57(16): 10183-10187

[13] Shyu FL, Lin MF. pi plasmons in two-dimensional arrays of aligned carbon nanotubes. Phys Rev B 1999; 60(20): 14434-14440

[14] Gommans HH, Alldredge JW, Tashiro H, Park J, Magnuson J, Rinzler AG. Fibers of aligned single-walled carbon nanotubes: Polarized Raman spectroscopy. J Appl Phys 2000; 88(5): 2509-2514

[15] Grüneis A, Saito R, Samsonidze GG, Kimura T, Pimenta MA, Jorio A, et al. Inhomogeneous optical absorption around the K point in graphite and carbon nanotubes. Phys Rev B 2003; 67(16): 165402-1-165402-7

[16] Grüneis A, Saito R, Jiang J, Samsonidze GG, Pimenta MA, Jorio A, et al. Resonant Raman spectra of carbon nanotube bundles observed by perpendicularly polarized light. Chem Phys Lett 2004; 387(4-6): 301-306.

[17] Kataura H, Kumazawa Y, Maniwa Y, Umezu I, Suzuki S, Ohtsuka Y, et al. Optical properties of single-wall carbon nanotubes. Synth Met 1999; 103(1-3): 2555-2558

[18] Haddon RC, Sippel J, Rinzler AG, Papadimitrakopoulos F. Purification and separation of carbon nanotubes. MRS Bullet 2004; 29: 252-259.

[19] Murakami Y, Chiashi S, Miyauchi Y, Hu MH, Ogura M, Okubo T, et al. Growth of vertically aligned single-walled carbon nanotube films on quartz substrates and their optical anisotropy. Chem Phys Lett 2004; 385 (3-4): 298-303

[20] Murakami Y, Einarsson E, Edamura T, Maruyama S. Polarization dependence of the optical absorption of single-walled carbon nanotubes. Phys Rev Lett 2005; 94 (8): 087402-1-087402-4.

[21] Murakami Y, Miyauchi Y, Chiashi S, Maruyama S. Direct synthesis of high-quality single-walled carbon nanotubes on silicon and quartz substrates. Chem Phys Lett 2003; 377 (1-2): 49-54

[22] Hu M, Murakami Y, Ogura M, Maruyama S, Okubo T. Morphology and chemical state of Co-Mo catalysts for growth of single-walled carbon nanotubes vertically aligned on quartz substrates. J Catalysis 2004; 225(1): 230-239

[23] Maruyama S, Kojima R, Miyauchi Y, Chiashi S, Kohno M. Low-temperature synthesis of high-purity single-walled carbon nanotubes from alcohol. Chem Phys Lett 2002; 360 (3-4): 229-234

[24] Murakami Y, Miyauchi Y, Chiashi S, Maruyama S. Characterization of single-walled carbon nanotubes catalytically synthesized from alcohol. Chem Phys Lett 2003; 374 (1-2): 53-58

[25] Murakami Y, Chiashi S, Miyauchi Y, Maruyama S. Direct synthesis of single-walled carbon nanotubes on silicon and quartz-based systems. Jpn J Appl Phys 2004; 43(3): 1221-1226

[26] Murakami Y, Einarsson E, Edamura T, Maruyama S. Polarization dependence of resonant Raman scattering from vertically aligned single-walled carbon nanotube films. Phys Rev B 2005, 71(8):085403-1-085403-8

[27] Jorio A, Saito R, Hafner JH, Lieber CM, Hunter M, McClure T et al. Phys Rev Lett 2001; 86(6): 1118-1121

[28] Maruyama S, Einarsson E, Murakami Y, Edamura T. Growth process of vertically aligned single-walled carbon nanotubes. Chem Phys Lett 2005; 403(4-6): 320-323

[29] Strano MS, Doorn SK, Haroz EH, Kittrell C, Hauge RH, Smalley RE. Assignment of (n, m) Raman and optical features of metallic single-walled carbon nanotubes. Nano Lett 2003; 3(8): 1091-1096

[30] Pichler T, Knupfer M, Golden MS, Fink J, Rinzler A, Smalley RE. Localized and delocalized electronic states in single-wall carbon nanotubes. 1998; 80(21): 4729-4732

[31] Reed BW, Sarikaya M. Electronic properties of carbon nanotubes by transmission electron energy-loss spectroscopy. Phys Rev B 2001; 64 (19): 195404-1-195404-13

[32] Taft EA, Philipp HR. Optical properties of graphite. Phys Rev 1965; 138(1A): A197-A202

[33] Kelly MK, Etchegoin P, Fuchs D, Kratschmer W, Fostiropoulos K. Optical-transitions of C-60 films in the visible and ultraviolet from spectroscopic ellipsometry. Phys Rev B 1992; 46(8): 4963-4968

[34] Marinopoulos AG, Reining L, Olevano V, Rubio A, Pichler T, Liu X, et al. Anisotropy and interplane interactions in the dielectric response of graphite. Phys Rev Lett 2002; 89(7): 076402-1-076402-4

[35] Borgheshi A, Guizzetti G. In: Handbook of Optical Constants of Solids II, edited by Palik ED, San Diego, USA: Academic Press Inc, 1991.

[36] Garcia-Vidal FJ, Pitarke JM. Optical absorption and energy-loss spectra of aligned carbon nanotubes. Euro Phys J B 2001; 22(2): 257-265

[37] Djurisic AB, Li EH. Optical properties of graphite. J Appl Phys 1999; 85(10): 7404-7410

[38] Venghaus H. Redetermination of dielectric function of graphite. Phys Stat Solidi B 1975; 71(2): 609-614.

[39] Kim Y, Minami N, Zhu W, Kazaoui S, Azumi R, Matsumoto M. Langmuir–Blodgett films of single-wall carbon nanotubes: layer-by-layer deposition and in-plane orientation of tubes. Jpn J Appl Phys 2003; 42(12): 7629-7634

[40] Lakowicz JR. Principles of Fluorescence Spectroscopy 2nd Ed., New York: Plenum Publishing Corp., 1999.

[41] Lee H, Kang TD, An KH, Bae DJ, Lee YH. Visible-ultraviolet polarized reflectivity spectra of anisotropically aligned single-walled carbon nanotube films. Jpn J Appl Phys 2003; 42(9A): 5880-5886

Figure captions

Fig. 1. Images of vertically aligned SWNT films taken at a fractured edge of the quartz substrate by FE-SEM. Strings seen in the images are bundles of SWNTs.

Fig. 2. HR-TEM images on a section of the aligned SWNT film. (a) Low magnification image on the top edge of the film and (b,c) high magnification images at the top edge of the film. (d) Magnified image from the other edge of the film section that presumably corresponds to the interface between the substrate and the film. Black circles correspond to catalyst used for SWNT growth.

Fig. 3. Raman scattering spectra measured from (a,b) vertically aligned and (c) 2D random SWNT films grown on quartz substrates with 488 nm laser incidence normal to the substrate. Spectrum (b) was measured at the spot where the alignment of SWNTs was mechanically perturbed by tweezers. Upper (Lower) panel correspond to RBM (TM) of the SWNTs. Asterisks denote RBM peaks observed only when the vertically aligned SWNTs are measured with incident light cross-polarized to the SWNT axis.

Fig. 4. Optical absorption spectra of SWNT films presented for (a) 0.5 - 3 eV with absolute absorbance and (b) 0.5- 6 eV with an arbitrary ordinate. The films were synthesized under various CVD chamber conditions with (i) high, (ii) medium, and (iii) low gas desorption rate V_{gd} from the CVD chamber wall. The sample measured in (iv) is a non-uniform SWNT film in which the film is partially aligned. The morphology of the film is denoted to each spectrum.

Fig. 5. Optical absorption spectra of a vertically aligned SWNT film 2.1 μm-thick per side (4.2 μm total thickness) measured with (a) s- and (b) p-polarization with respect to the substrate. The incident angle of the light is varied from normal incidence θ = 0° (bottom spectrum) to θ = 45° (uppermost spectrum) at a step of 7.5°. All spectra are normalized by the $\cos^{-1}\theta$ increment of the light path length. Dotted vertical lines indicate locations of inter-subband absorption of E^{S}_{11}, E^{S}_{22}, E^{M}_{11} and absorption peaks at 4.5 eV and 5.25 eV. The measured film is identical to that shown as "180 s" in Fig. 9.

Fig. 6. Illustration of the coordinates (x, y, z) and angles (θ, φ, ψ, ζ) used in the formulation of the anisotropic optical absorption of light propagating along $\boldsymbol{k}$ by a SWNT with axial vector $\boldsymbol{l}$.

Fig. 7. (a) Part of the measured absorption spectra presented in Fig. 5b for 0.5 - 3 eV by p-polarization from θ = 0° to 45° at a step of 7.5° (solid lines) and its extrapolation to the case of θ = 90° (dashed line). (b) Calculated anisotropy α from Eq. 11 for the same energy range.

Fig. 8. (a) Fitting of the measured absorption spectra presented in Fig. 5b from θ = 0° to 45° at a step of 7.5° by four Lorentzian curves, whose peak locations and widths are given in the text. Arrows indicate the direction of change of each Lorentzian component from θ = 0° to 45°. Dotted lines overlapping the measured spectra represent the sum of these Lorentzian curves. (b) Lorentzian curve fitting performed on a randomly oriented SWNT film corresponds to spectrum (iii) in Fig. 4, using the same peak position and widths. (c) Bare absorption cross-section for parallel ($\sigma_{\parallel}$, solid line) and perpendicular polarization ($\sigma_{\perp}$, dashed line) calculated with Eqs. 14 and 15.

Fig. 9. Cross-sectional FE-SEM images of vertically aligned SWNT films with CVD reaction times of 15, 30, 60, 180, and 600 s.

Fig. 10. Changes of (a) optical absorbance of the SWNT film at 2.54 eV measured with normal light incidence ($\theta = 0$) divided by the film thickness measured by FE-SEM, and (b) the ratio of magnitudes of Lorentzian-fitted curves at 4.5 and 5.25 eV, according to CVD reaction time.

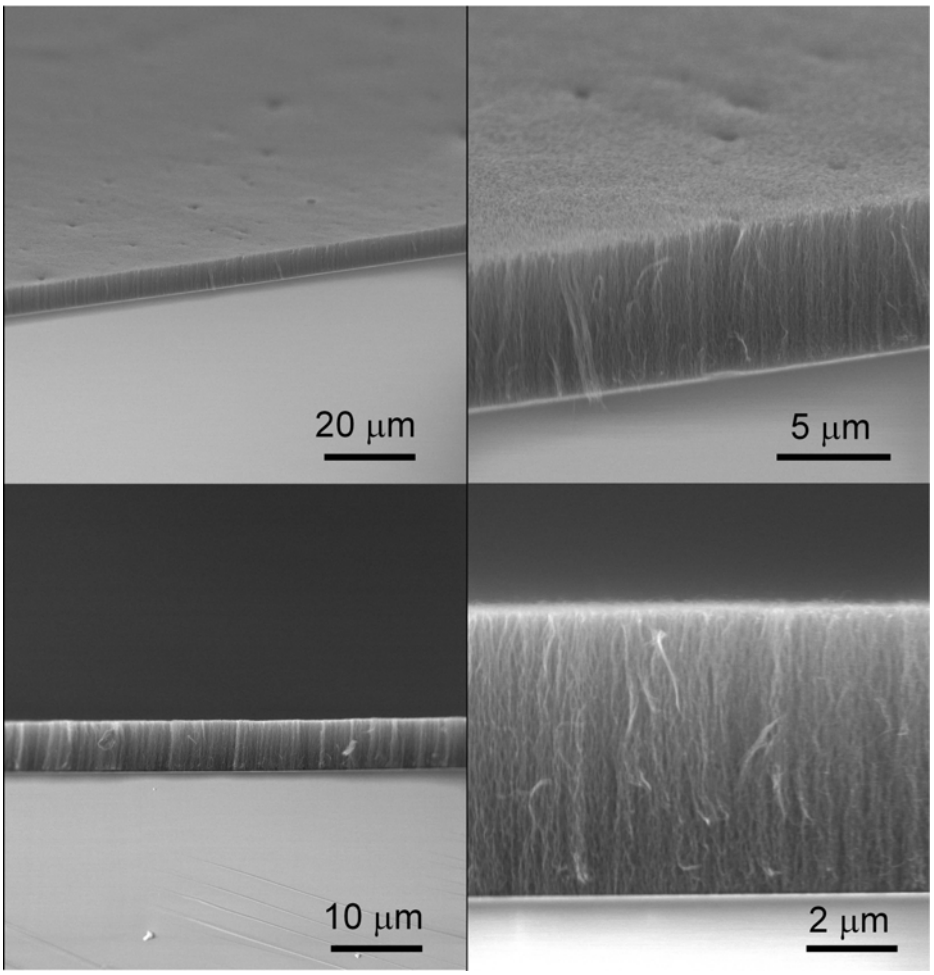

Figure 1

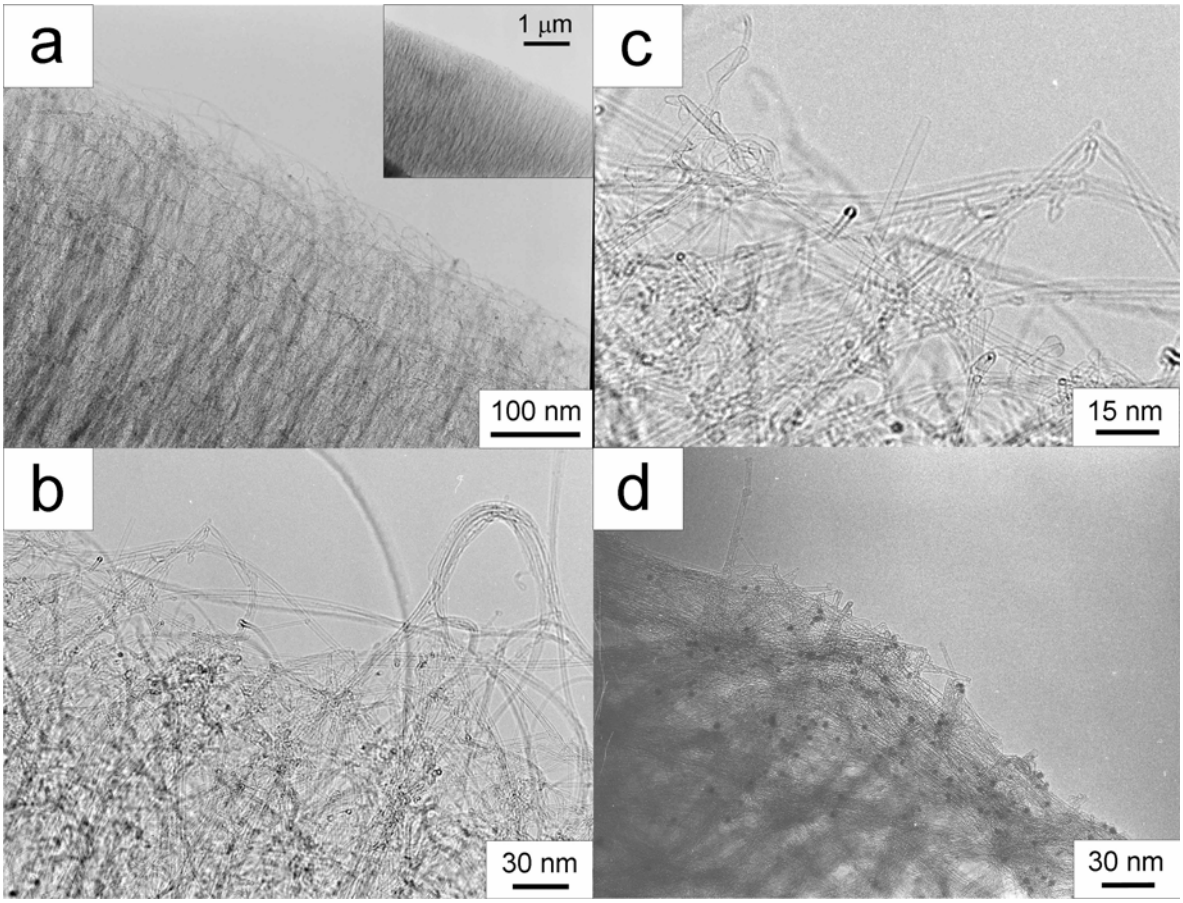

Figure 2

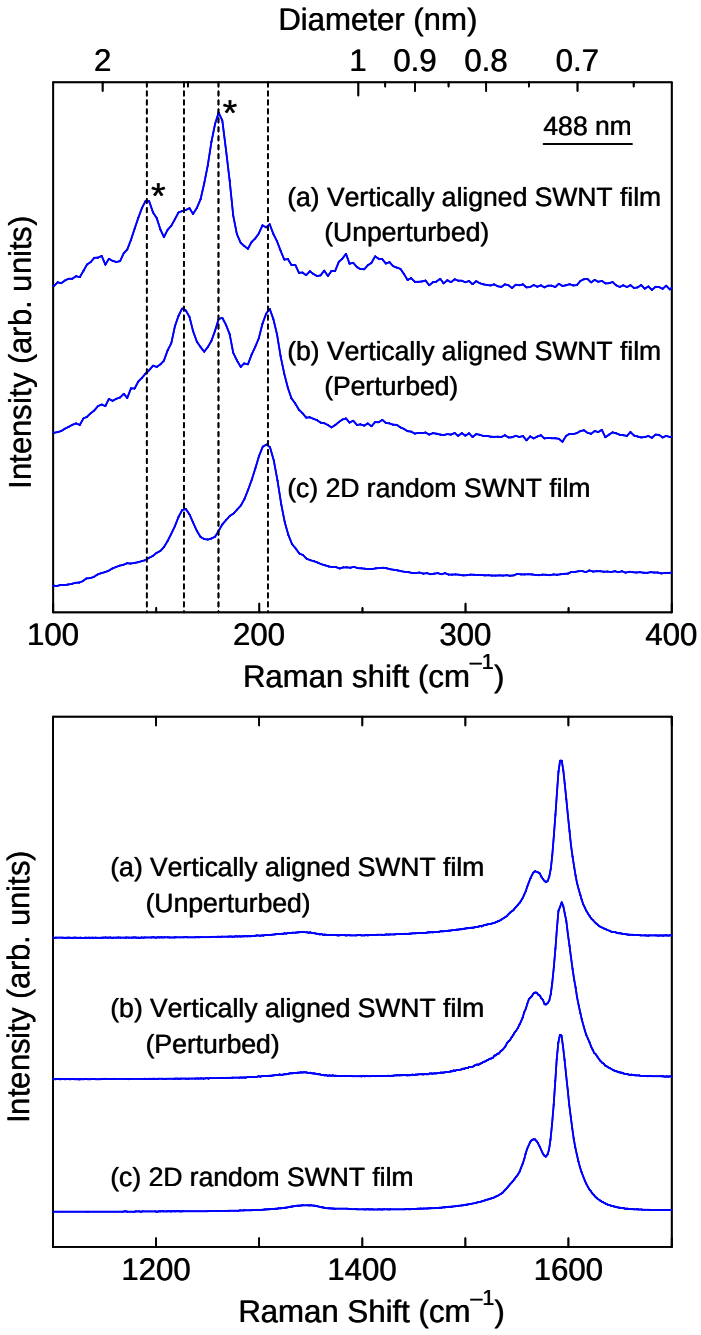
Diameter (nm)
2
1
0.9
0.8
0.7
488 nm
(a) Vertically aligned SWNT film
(Unperturbed)
(b) Vertically aligned SWNT film
(Perturbed)
(c) 2D random SWNT film
Intensity (arb. units)
100
200
300
400
Raman shift (cm^{-1})
(a) Vertically aligned SWNT film
(Unperturbed)
(b) Vertically aligned SWNT film
(Perturbed)
(c) 2D random SWNT film
Intensity (arb. units)
1200
1400
1600
Raman Shift (cm^{-1})

Figure 3

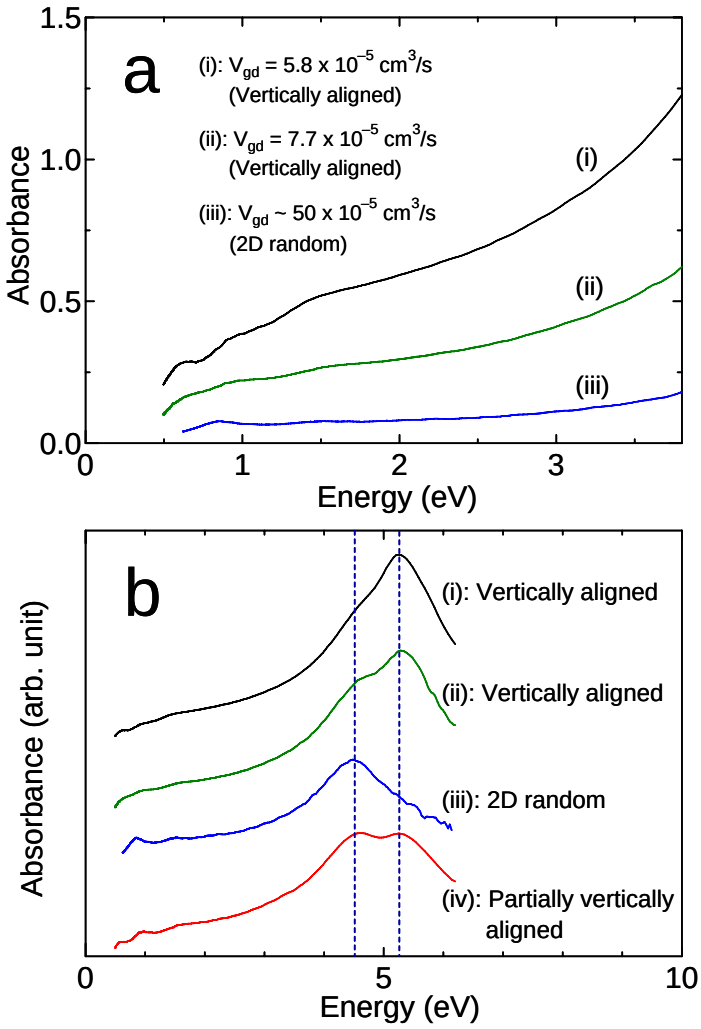
a
(i): V_{gd} = 5.8 x 10^{-5} cm^3/s
(Vertically aligned)
(ii): V_{gd} = 7.7 x 10^{-5} cm^3/s
(Vertically aligned)
(iii): V_{gd} ~ 50 x 10^{-5} cm^3/s
(2D random)
(i)
(ii)
(iii)
Absorbance
Energy (eV)
b
(i): Vertically aligned
(ii): Vertically aligned
(iii): 2D random
(iv): Partially vertically aligned
Absorbance (arb. unit)
Energy (eV)

Figure 4

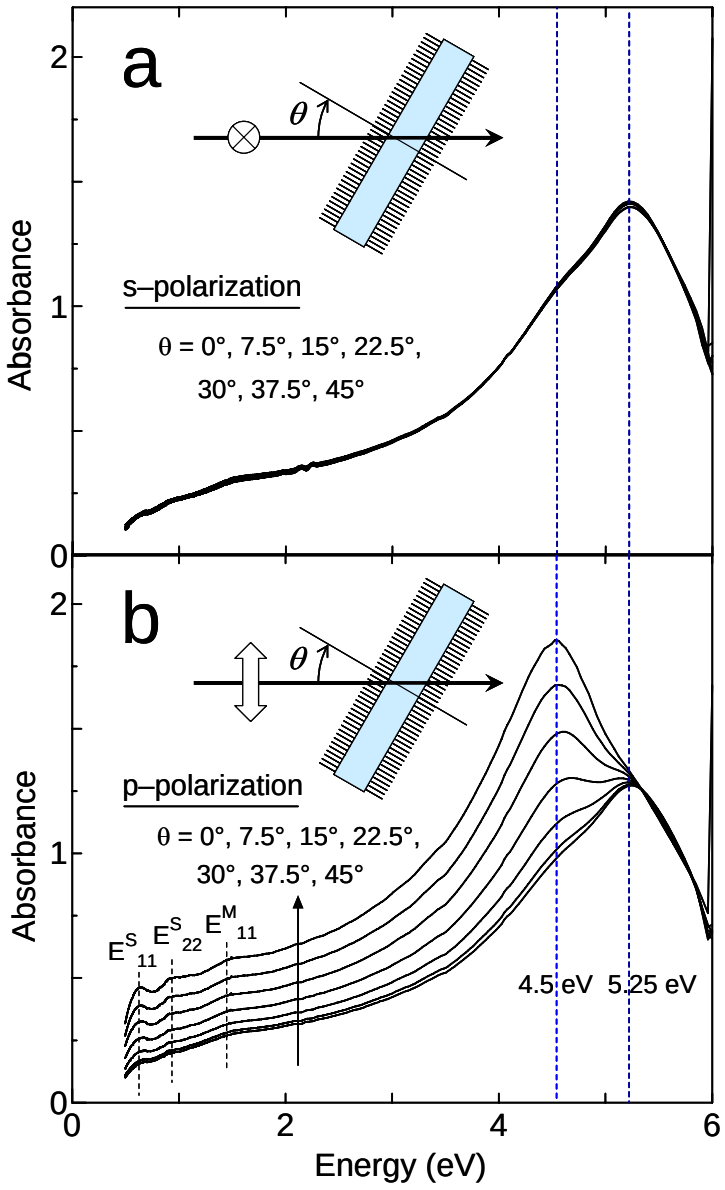
a
θ
s–polarization
θ = 0°, 7.5°, 15°, 22.5°,
30°, 37.5°, 45°
Absorbance
b
θ
p–polarization
θ = 0°, 7.5°, 15°, 22.5°,
30°, 37.5°, 45°
E^S_11 E^S_22 E^M_11
4.5 eV 5.25 eV
Absorbance
Energy (eV)
0
1
2
0
2
4
6

Figure 5

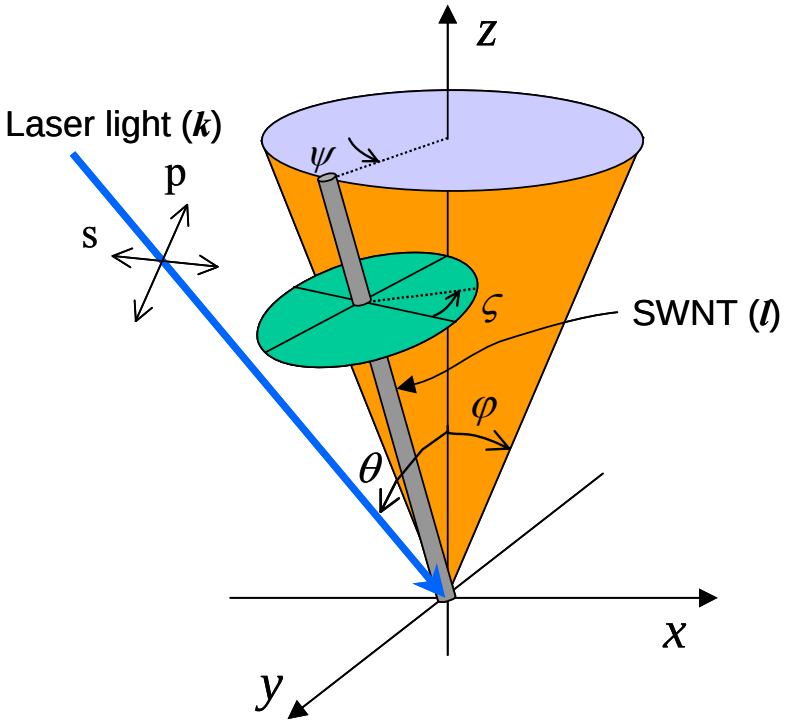

Figure 6

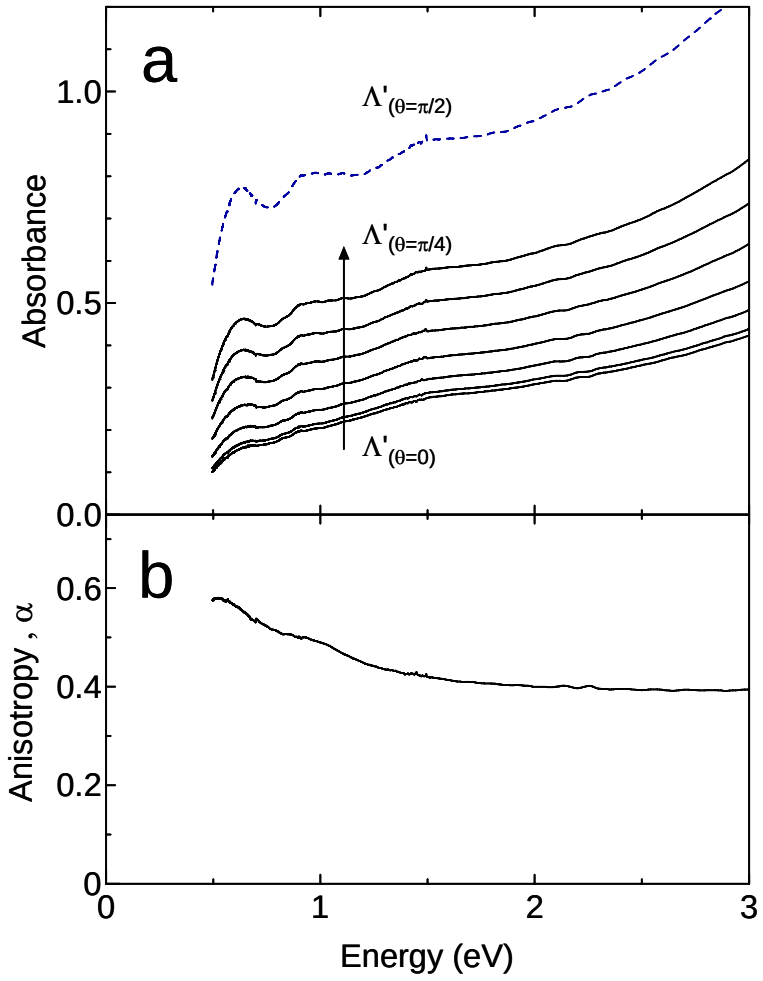
a
b
Absorbance
Anisotropy , α
Energy (eV)
Λ'(θ=π/2)
Λ'(θ=π/4)
Λ'(θ=0)
1.0
0.5
0.0
0.6
0.4
0.2
0
0
1
2
3

Figure 7

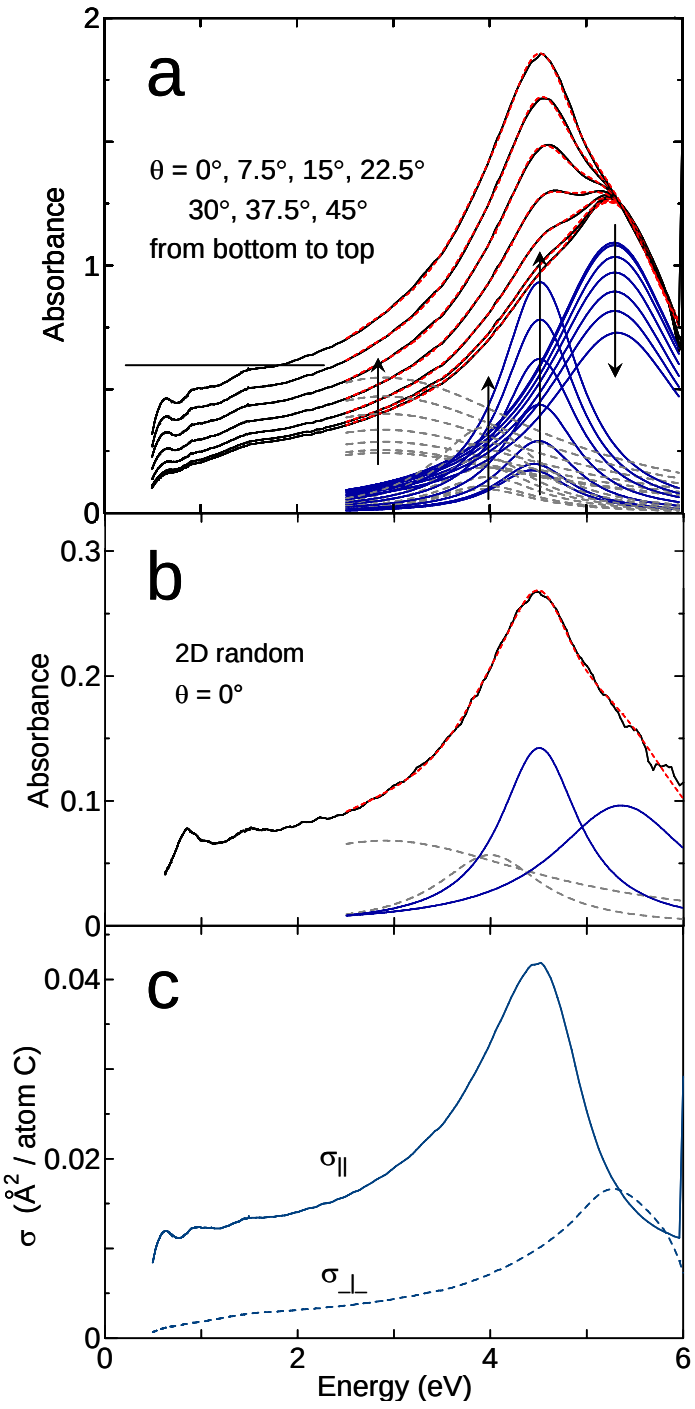
a
θ = 0°, 7.5°, 15°, 22.5°
30°, 37.5°, 45°
from bottom to top
Absorbance
b
2D random
θ = 0°
Absorbance
c
σ (Å² / atom C)
σ||
σ⊥
Energy (eV)

Figure 8

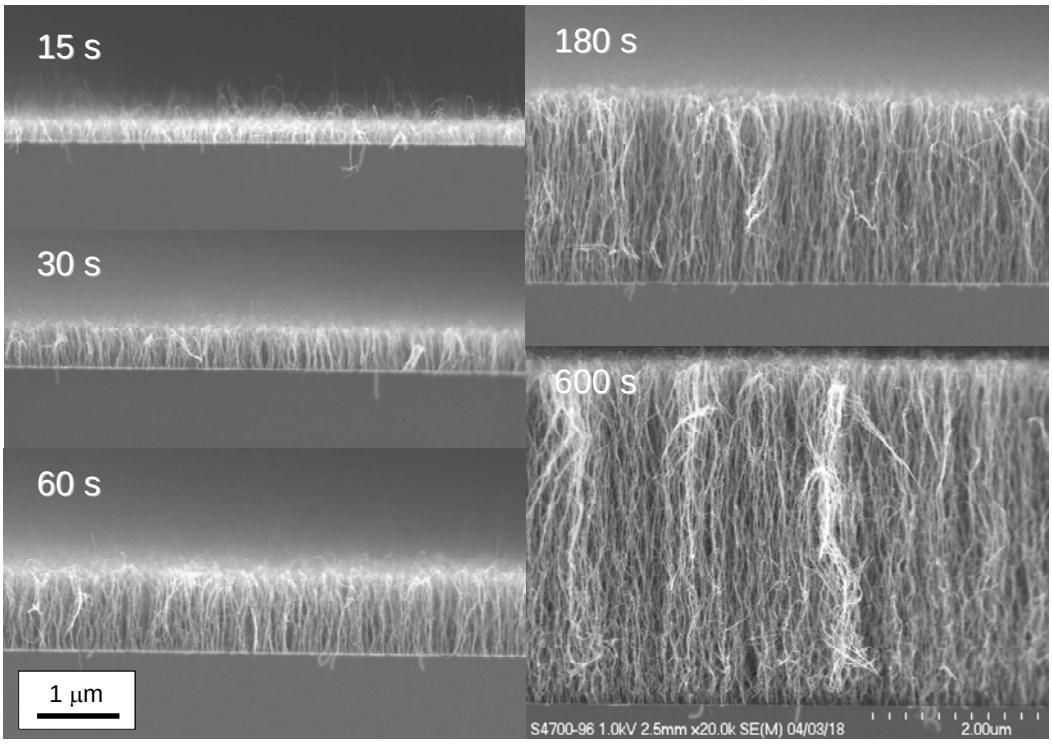
15 s
30 s
60 s
180 s
600 s
1 μm
S4700-96 1.0kV 2.5mm x20.0k SE(M) 04/03/18
2.00um

Figure 9

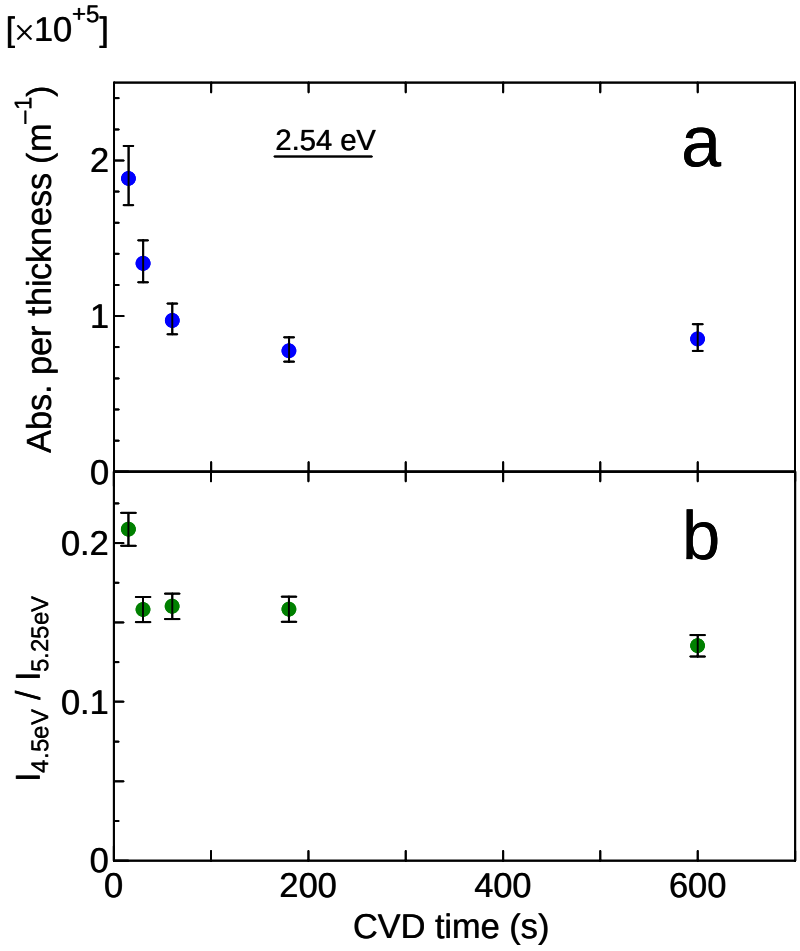
[×10+5]
Abs. per thickness (m−1)
2.54 eV
a
2
1
0
b
0.2
0.1
0
I4.5eV / I5.25eV
0
200
400
600
CVD time (s)

Figure 10